

The Inert Dark Matter

Ethan M. Dolle*, Shufang Su†

Department of Physics, University of Arizona, Tucson, AZ 85721

Abstract

The lightest neutral scalar in the Inert Higgs Doublet Model is a natural candidate for WIMP dark matter. In this paper, we analyzed the dark matter relic density in the Inert Higgs Doublet model. Various theoretical and experimental constraints are taken into account. We found that there are five distinctive regions that could provide the right amount of the relic density in the Universe. Four out of those five regions have a light particle spectrum which could be studied at the Large Hadron Collider.

* edolle@physics.arizona.edu

† shufang@physics.arizona.edu

I. INTRODUCTION

About 20% of the Universe is made of cold dark matter. The origin of the dark matter, however, still remains a mystery. While the Standard Model (SM) of particle physics has been very successful in explaining the data from almost all of the particle physics experiments to date, none of the SM particles can be a good candidate for the dark matter. Its existence provides unambiguous evidence for new physics beyond the Standard Model.

A Weakly Interacting Massive Particle (WIMP) is a promising candidate for the dark matter, given that the WIMP relic density is naturally around the observed value [1]

$$\Omega h^2 = 0.112 \pm 0.009, \quad (1)$$

for a WIMP mass around the electroweak scale ~ 100 GeV. WIMPs also appear naturally in many beyond the Standard Model scenarios. One popular candidate is the lightest neutralino in supersymmetric models, which provides an example of spin-1/2 WIMP dark matter. Spin-1 WIMP dark matter has been studied in the framework of extra dimension models, for example, the lightest Kaluza-Klein photon in Universal Extra Dimension models [2].

Spin-0 dark matter has been studied [3, 4, 5] in the framework of the SM plus an extra scalar. The minimal model includes an extra real scalar gauge singlet S that is charged under a Z_2 symmetry. The only renormalizable couplings are the quartic self-coupling $\lambda_S S^4$ and the Higgs- S coupling $\lambda S^2 H^\dagger H$. It was shown that for a SM Higgs with mass in the range of $100 \text{ GeV} \leq m_h \leq 200 \text{ GeV}$ and dark matter with mass in the range of $10 \text{ GeV} \leq m_S \leq 100 \text{ GeV}$, viable regions of parameter space exists for the dark matter candidate S to provide the right amount of relic density in the Universe [5].

Unlike the WIMP, the mass and the couplings of such a scalar dark matter particle often needs to be fine tuned to be consistent with the observed dark matter relic density. WIMP-type scalar dark matter could appear in a simple extension of the SM with the addition of a Higgs $SU(2)_L$ doublet. Unlike the SM Higgs doublet, which couples to both fermion and gauge sectors, such an extra scalar doublet is *inert* in the sense that it couples to gauge bosons only. Such inertness can be guaranteed by imposing a discrete Z_2 parity. The lightest inert particle (LIP) is therefore stable. If it is neutral, it can be a good WIMP dark matter candidate.

The Inert Higgs Doublet Model (IHDM)¹ was first proposed in the late 70's [6]. It has received recent attention [7] since it could be used to solve the naturalness problem in the Standard Model. With a splitting in the masses of the neutral and charged components of the inert Higgs fields, the resulting positive contribution to the oblique T parameter allows this model to accommodate a SM Higgs with a much heavier mass. Such an inert Higgs sector also appears in the recently proposed left-right Twin Higgs model [8]. In addition, an inert Higgs doublet (or doublets) could be used to explain the small Majorana neutrino

¹ Strictly speaking, the extra $SU(2)_L$ scalar doublet is not a Higgs doublet since it does not obtain a vacuum expectation value. Such model is also referred to as “Inert Scalar Doublet Model” in the literature.

mass via the one-loop radiative seesaw mechanism [9], electroweak symmetry breaking [10], grand unification [11] and leptogenesis [12].

There have been some studies on the dark matter candidate in the IHDM. Ref. [13] studied the dark matter relic density in the IHDM in certain regions of parameter space. The right amount of relic density could be obtained for dark matter with mass around 40 GeV – 80 GeV or larger than 600 GeV. Ref. [14, 15] studied the neutrino signatures from dark matter annihilation. The continuous gamma ray spectrum from fragmentation and monochromatic gamma ray lines were studied in Ref. [13] and [16] respectively. Positron and antiproton signatures were studied in Ref. [17]. Direct detection has been studied in [7, 13, 18]. There is also a collider analysis based on the LEP II limit [19] as well as collider signatures of SA associated production with $A \rightarrow Sl^+l^-$ at the Large Hadron Collider (LHC) [20].

In this work, we performed a complete analysis of the dark matter relic density in the IHDM over the whole parameter space, taking into account various theoretical and experimental constraints. The latest results of the collider constraints based on supersymmetric process $e^+e^- \rightarrow \chi_1^0\chi_2^0$ search at the LEP II are imposed [19]. Unlike Ref. [13], in which only a low SM Higgs mass $m_h = 120$ GeV and 200 GeV are considered, our analysis also includes studies with a high SM Higgs mass $m_h = 500$ GeV. In Ref. [13], the mass splittings between H^\pm , A and the dark matter candidate S , $(m_{H^\pm} - m_S, m_A - m_S)$, are fixed to be (50, 10) GeV and (10, 5) GeV for the low and high dark matter mass regions, respectively. We study cases when the mass splittings between H^\pm , A and S are small, in which coannihilations play an important role, as well as cases when the mass splittings are large. In regions that overlap with those analyzed in Ref. [13], our results agree with the literature. We identify additional regions of parameter space, in which the dark matter relic density is also consistent with the WMAP result but were overlooked previously. We also present our results in the parameter spaces of physical Higgs masses and Higgs couplings, which are convenient to use for studies of collider phenomenology and dark matter detections.

The rest of the paper is organized as follows. In Sec. II, we briefly present the IHDM. In Sec. III, we discuss the theoretical and experimental constraints on the model parameter space. In Sec. IV, we present our results of the relic density analysis. In Sec. V, we conclude.

II. THE INERT HIGGS DOUBLET MODEL

The IHDM is an extension of the Higgs sector of the SM. Besides the usual Higgs doublet $H_1 = H_{\text{SM}}$, an additional Higgs doublet H_2 is introduced:

$$H_2 = \begin{pmatrix} H^+ \\ (S + iA)/\sqrt{2} \end{pmatrix}, \quad (2)$$

which is charged under $SU(2)_L \times U(1)_Y$ as $(\mathbf{2}, 1/2)$. Unlike the SM Higgs boson, which couples to both SM gauge bosons and matter fermions, the extra Higgs doublet H_2 couples to the gauge sector only. Such couplings can be guaranteed by imposing a Z_2 symmetry

(sometimes also called matter parity) under which all particles except H_2 are even. In particular, under the Z_2 symmetry:

$$H_1 \rightarrow H_1, \quad H_2 \rightarrow -H_2. \quad (3)$$

While H_1 obtains a vacuum expectation value (VEV) $v/\sqrt{2} = 174$ GeV as in the SM, H_2 does not obtain a VEV: $\langle H_2 \rangle = 0$. The Z_2 symmetry is, therefore, not spontaneously broken. The lightest particle in H_2 is stable and could be a good dark matter candidate.

The most general CP-conserving potential in the Higgs sector that respects the Z_2 symmetry can be written as

$$V = \mu_1^2 |H_1|^2 + \mu_2^2 |H_2|^2 + \lambda_1 |H_1|^4 + \lambda_2 |H_2|^4 + \lambda_3 |H_1|^2 |H_2|^2 + \lambda_4 |H_1^\dagger H_2|^2 + \left[\frac{\lambda_5}{2} (H_1^\dagger H_2)^2 + h.c. \right]. \quad (4)$$

Notice that the usual mixing term $\mu_{12}^2 H_1^\dagger H_2$ is forbidden by the Z_2 symmetry. After electroweak symmetry breaking, three degrees of freedom in H_1 are eaten by massive gauge bosons W^\pm and Z . We are left with one physical Higgs boson h , which resembles the SM Higgs boson, as well as four inert scalars: the CP even one S , the CP odd one A and a pair of charged ones H^\pm . The mass of h is related to λ_1 via

$$m_h^2 = -2\mu_1^2 = 2\lambda_1 v^2. \quad (5)$$

The masses of S , A and H^\pm are related to parameters in the Higgs potential as

$$m_{H^\pm}^2 = \mu_2^2 + \lambda_3 v^2/2, \quad (6)$$

$$m_S^2 = \mu_2^2 + (\lambda_3 + \lambda_4 + \lambda_5)v^2/2, \quad (7)$$

$$m_A^2 = \mu_2^2 + (\lambda_3 + \lambda_4 - \lambda_5)v^2/2. \quad (8)$$

$$(9)$$

We define the mass differences δ_1 and δ_2 as

$$\delta_1 = m_{H^\pm} - m_S = -\frac{(\lambda_4 + \lambda_5)v^2}{2(m_{H^\pm} + m_S)}, \quad \delta_2 = m_A - m_S = -\frac{\lambda_5 v^2}{(m_A + m_S)}. \quad (10)$$

It is obvious that λ_4 and λ_5 control the mass splitting between the charged and neutral CP even states, while λ_5 also controls the mass splitting between the CP odd and CP even states. In our analysis below, we assume that the CP even scalar S is the LIP, therefore the dark matter candidate, giving $\delta_{1,2} > 0$. The numerical results of the relic density analysis are similar if A is the LIP dark matter.

The Higgs potential in Eq. (4) has seven parameters:

$$(\mu_1^2, \mu_2^2, \lambda_1, \lambda_2, \lambda_3, \lambda_4, \lambda_5). \quad (11)$$

They could be replaced by the Higgs VEV v , physical Higgs masses, mass splittings, and a sum of quartic couplings $\lambda_L = \lambda_3 + \lambda_4 + \lambda_5$ as

$$(v, m_h, m_S, \delta_1, \delta_2, \lambda_2, \lambda_L). \quad (12)$$

In particular, λ_L shows up in the couplings of SSh and $SShh$, which is relevant for dark matter annihilation. It is therefore convenient to pick λ_L as a model parameter. The quartic coupling λ_2 only shows up in self-couplings involving S , A and H^\pm . It does not play an important role for the dark matter analysis that we present below.

III. THEORETICAL AND EXPERIMENTAL CONSTRAINTS

There are various experimental constraints on the IHDM from direct collider searches, indirect electroweak precision test and dark matter direct detections.

- **W and Z decay widths**

Light H^\pm , S and A could lead to deviations of Z and W decay widths from the SM value. On the other hand, $\Gamma_{W,Z}$ have been measured precisely at the LEP and the Tevatron [21], which agree well with SM predictions. Therefore regions in which the decay processes $W^\pm \rightarrow SH^\pm/AH^\pm$ and $Z \rightarrow H^+H^-/SA$ are kinematically allowed have already been excluded. These translate into constraints for m_S and $\delta_{1,2}$ as

$$\begin{aligned} 2m_S + \delta_1 &> m_W, & 2m_S + \delta_1 + \delta_2 &> m_W, \\ 2m_S + 2\delta_1 &> m_Z, & 2m_S + \delta_2 &> m_Z. \end{aligned} \tag{13}$$

- **Direct collider searches**

Light neutral and charged Higgses have been searched for at the LEP and the Tevatron. Limits from conventional searches for H^\pm , S and A , however, do not apply for Higgses in the IHDM since those searches rely on decays of Higgses into fermion pairs and/or Higgs production via top quark decay. Neutral and charged Higgses in the IHDM, on the other hand, do not couple to fermions. In particular, the charged Higgs has been searched for at the LEP and the Tevatron [22, 23]. A lower mass bound of 74 – 79 GeV at 95% C.L. is obtained at the LEP [22] considering $H^+ \rightarrow c\bar{s}, \tau^+\nu$. A more recent search at CDF [23] studied the charged Higgs produced in the top quark decay $t \rightarrow H^+b$, with H^+ further decaying into a pair of quarks, leptons, or $W^+\phi$. The bounds on the charged Higgs mass from those searches do not apply to Higgses in the IHDM since Higgs-fermion-fermion couplings are absent.

Experimental signatures for S , A and H^\pm , however, is similar to those of neutralinos and charginos in the Minimal Supersymmetric Standard Model (MSSM), as S appears as missing energy at colliders, similar to the lightest supersymmetric particle(LSP) in the MSSM. In particular, searches of $e^+e^- \rightarrow \chi_1^0\chi_2^0$ at the LEP II can be interpreted as searches for $e^+e^- \rightarrow SA$. Therefore, the null result for neutralino and chargino searches at the LEP II can be used to set limits on m_{H^\pm} , m_A and m_S in the IHDM. A recent analysis [19] argued that a direct application of the upper limit on the LEP II $\chi_1^0\chi_2^0$ cross section to the IHDM is oversimplified due to the difference between the MSSM process $\chi_1^0\chi_2^0$ and IHDM process SA . Based on DELPHI analyses of $e^+e^- \rightarrow \chi_1^0\chi_2^0$ with $\chi_2^0 \rightarrow \chi_1^0q\bar{q}, \mu^+\mu^-, e^+e^-$, Ref. [19] determined the efficiencies for the corresponding MSSM and IHDM processes after cuts using

Monte-Carlo simulations. The ratio of the efficiencies is then used to rescale the MSSM cross section upper limit and applied to the IHDM. It is shown that regions satisfying $m_S \lesssim 80$ GeV, $m_A \lesssim 100$ GeV and $\delta_2 > 8$ GeV are excluded by LEP II MSSM searches. This limit is stronger than previous estimations by the direct application of the $\chi_1^0 \chi_2^0$ cross section upper limit to the IHDM [7, 24]. For $\delta_2 < 8$ GeV, however, limits on scalar masses are much weaker, due to the small mass splitting and the resulting soft jets and leptons in the final states. For $\delta_2 < 8$ GeV, only the LEP I limit, $m_S + m_A > m_Z$, applies.

Similarly, searches of the supersymmetric channel $e^+e^- \rightarrow \chi_1^+ \chi_1^-$ at the LEP II [25] can be used to set a bound on m_{H^\pm} . Taking into account the cross section difference of scalars versus fermions, a limit of $m_{H^\pm} \gtrsim 70 - 90$ GeV can be derived from the LEP II chargino searches [24].

- **Electroweak precision test (EWPT)**

Electroweak precision measurements provide strong constraints for any new physics beyond the SM. In the global electroweak precision fit to the SM, a light Higgs is preferred: $m_h = 90_{-27}^{+36}$ GeV, with $m_h < 163$ GeV at 95% C.L. [26]. Oblique parameters [27] S , T and U are often used to parameterize radiative correction to gauge boson propagators. A heavier SM Higgs contributes positively to S while negatively to T . Extra Higgs bosons in the IHDM, namely H^\pm , S and A , also contribute to the S and T parameters, which could possibly cancel the effect of a heavy SM Higgs boson [7]. Therefore, a heavy SM Higgs can be accommodated in the IHDM. In our analysis, we require the overall contribution to the S and T parameters from extra scalars in the IHDM to fall within the 68% C.L. ellipse in $S-T$ plane. Since we considered possible large mass splittings $\delta_{1,2}$, where the approximate formulas for ΔS and ΔT in Ref. [7] might not be valid, we used the full expressions for the contributions to ΔS and ΔT for a Higgs doublet [7] when imposing this constraint.

Fig. 1 shows the allowed region for mass splittings δ_1 and δ_2 given the constraints on the oblique parameters S and T from electroweak precision measurements, for several different choices of m_S . The dependence on m_S is small, especially for large $\delta_{1,2}$. For $m_h = 120$ GeV (left plot), the allowed region falls along the diagonal direction of $\delta_1 \sim \delta_2$. The mass splittings $\delta_{1,2}$ could both be large as long as these two mass splittings are close to each other. For $m_h = 500$ GeV (right plot), a large contribution from the inert Higgs doublet is needed to cancel the large positive S and negative T contribution from a heavy SM Higgs boson. Therefore, the value for δ_1 is constrained to be quite large $\delta_1 \gtrsim 150$ GeV, while the value for δ_2 could still be as small as 0.

- **Dark matter detection**

Dark matter direct detection excluded spin-independent dark matter–nuclei scattering cross section up to about 10^{-43}cm^2 at 90% C.L. [28, 29], which is 7–8 orders of magnitude larger than dark matter – nucleon scattering via Z exchange. This limit, however, can be easily avoided by introducing a small mass splitting between S and

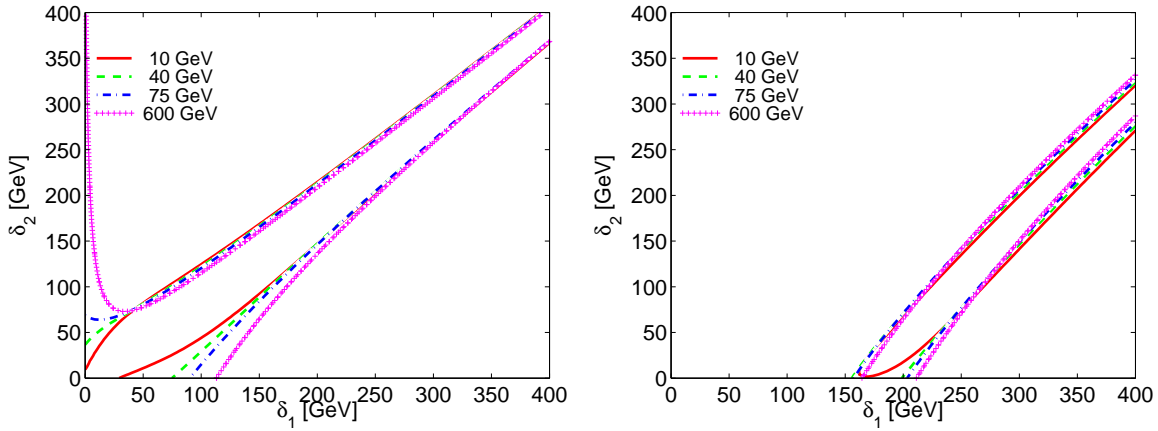


FIG. 1: Plot of the 68% C.L. allowed region in mass splittings δ_1 and δ_2 given the constraints on S and T from precision electroweak measurements. The value for the SM Higgs mass is set to be 120 GeV for the left plot and 500 GeV for the right plot. m_S is taken to be 10 GeV (solid curve), 40 GeV (dashed curve), 75 GeV (dash-dotted curve) and 600 GeV (dotted curve).

A: $\delta_2 \gtrsim$ a few hundred KeV, given the typical kinetic energy of the dark matter and the momentum transfer between the dark matter and the scattering nuclei in such scattering processes.

The spin-independent dark matter–nucleon scattering cross section via SM h -exchange is given by [7]

$$\sigma = \frac{1}{4\pi} \left(\frac{m_r m_N}{m_S} \right)^2 \left(\frac{\lambda_L f}{m_h^2} \right)^2 \quad (14)$$

where m_N is the nucleon mass, m_r is the reduced mass of the dark matter–nucleon pair, and f is used to parameterize the nucleonic matrix element. The typical range for f is taken to be 0.14 – 0.66 [30]. In our analysis, we take f to be 0.14 to be on the safe side. Latest results from XENON10, CDMS, CRESST, CoGeNT and TEXONO are used in our analysis [28, 29, 31, 32, 33, 34]. Portions of parameter space in small m_S , m_h and large $|\lambda_L|$ region are excluded by the upper limits on the spin-independent dark matter–nucleon cross section.

The bounds from indirect dark matter detection (gamma rays, for example) is weak in the IHDM. Moreover, those bounds are subject to large astrophysical uncertainties involved in those observations. Therefore, we don't consider constraints from indirect dark matter detections.

In addition, we impose the following theoretical constraints.

- **Vacuum stability**

We require the vacuum stability of the Higgs potential at tree level, which leads to

$$\lambda_{1,2} > 0, \tag{15}$$

$$\lambda_3, \lambda_3 + \lambda_4 - |\lambda_5| > -2\sqrt{\lambda_1\lambda_2}. \tag{16}$$

- **Perturbativity**

We require that corrections to the beta function of λ_1 from non-SM quartic couplings $\lambda_{3,4,5}$ is less than the 50% of the SM term $24\lambda_1^2$ [7]. This amounts to the constraint:

$$\lambda_3^2 + (\lambda_3 + \lambda_4)^2 + \lambda_5^2 < 12\lambda_1^2. \tag{17}$$

The evolution of the remaining quartic couplings does not lead to extra constraints. In addition, we require the quartic coupling λ_2 to be in the perturbativity region:

$$\lambda_2 < 1. \tag{18}$$

IV. RELIC DENSITY ANALYSIS

We analyzed the relic density in the IHDM using the program MicrOMEGAs [35]. This program solves the Boltzmann equation numerically, using the program CalcHEP [36] to calculate all of the relevant cross sections. When the mass splittings between the dark matter candidate and other particles are small, coannihilation effects are also included.

In our analysis, we fixed the SM Higgs mass to be 120 GeV (preferred by the EWPT in the SM) or 500 GeV (preferred by naturalness, and could be consistent with the EWPT with large splittings between H^\pm , S and A). We fixed $\lambda_2 = 0.1$ since it does not enter into the dark matter relic density analysis. We studied both the cases of small mass splittings and large mass splittings. When $\delta_1(\delta_2)$ is small, coannihilation between S and $H^\pm(A)$ is important. Part of our study overlaps with the analysis in Ref. [13], which, only considered small Higgs masses $m_h = 120$ GeV and 200 GeV with fixed mass splittings $(\delta_1, \delta_2) = (50, 10)$ GeV for the low mass region and $(\delta_1, \delta_2) = (10, 5)$ GeV for the high mass region. Results in Ref. [13] were presented in $\mu_2 - m_S$ plane. We present our results in $\lambda_L - m_S$ plane instead, which is more transparent since m_S and λ_L are the two relevant parameters for the dark matter analysis, as well as studies of dark matter direct and indirect detections. In particular, the value of λ_L is closely related to the neutrino and gamma ray flux from dark matter annihilation, and the cross section for dark matter–nucleon scattering. Larger λ_L typically leads to enhanced flux and increased dark matter–nucleon scattering cross sections, and the inert Higgs dark matter has a better chance to be detected at future dark matter detection experiments.

We discuss below in detail two mass regions of m_S that could provide the amount of dark matter relic density consistent with the WMAP result at the 3σ level: (A) low mass region where $m_S < 100$ GeV, and (B) high mass region where 400 GeV $< m_S <$ around a TeV.

A. Low mass region

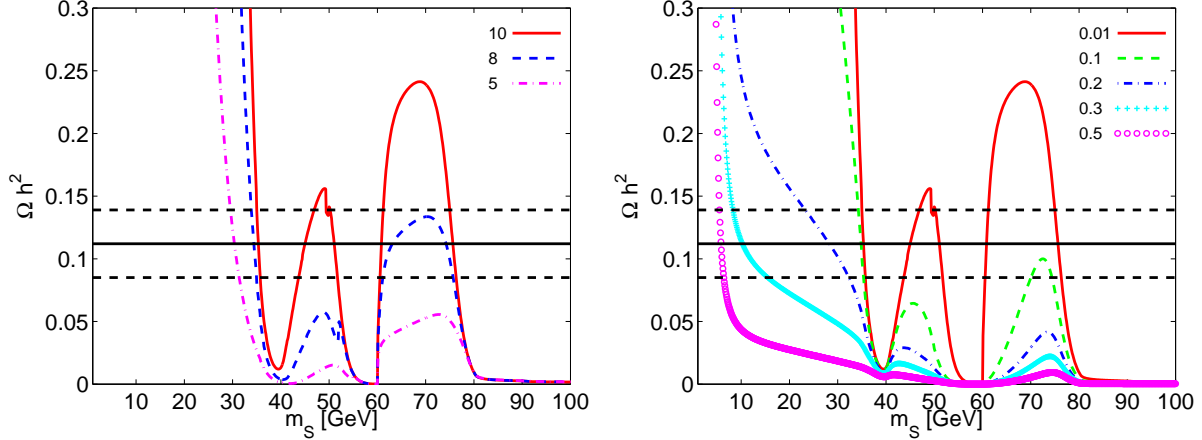


FIG. 2: Dependence of the relic density on m_S for $m_h=120$ GeV and $\delta_1 = 50$ GeV. In the left plot, δ_2 is chosen to be 10 GeV (solid line), 8 GeV (dashed line) and 5 GeV (dash-dotted line) while λ_L is fixed to be 0.01. In the right plot, λ_L is chosen to be 0.01 (solid line), 0.1 (dashed line), 0.2 (dash-dotted line), 0.3 “+” line), 0.5 (“o” line) while δ_2 is fixed to be 10 GeV. The horizontal band indicates the 3σ region that is consistent with relic density measurement from WMAP: $0.085 < \Omega h^2 < 0.139$.

To illustrate the dependence of the relic density Ωh^2 on m_S , λ_L and mass splittings $\delta_{1,2}$, we present in Fig. 2 curves of Ωh^2 vs. m_S for various choices of δ_2 (left plot) and λ_L (right plot). The horizontal band indicates the 3σ region that is consistent with relic density measurement from WMAP: $0.085 < \Omega h^2 < 0.139$. A light SM Higgs mass $m_h = 120$ GeV is used in both plots.

The red curve in the left plot of Fig. 2 corresponds to $(\delta_1, \delta_2) = (50, 10)$ GeV. Therefore, coannihilation between S and A is important while coannihilation between S and H^\pm is not. For small m_S , $SS \rightarrow b\bar{b}$ via SM h exchange dominates, with cross section proportional to λ_L^2 . The cross section is typically small due to the small bottom Yukawa coupling, which leads to relic density too big that overcloses the Universe. When m_S gets larger, $SA \rightarrow q\bar{q}$ via Z exchange becomes more and more important. The relic density enters the WMAP 3σ region for m_S around 35 GeV. The coannihilation cross section maximizes at the Z -pole: $m_S + m_A \sim m_Z$, corresponding to the dip around $m_S \sim 40$ GeV. The coannihilation cross section decreases when m_S increases away from the Z -pole region, which makes the relic density falls back to the allowed region. As m_S gets larger, $SS \rightarrow b\bar{b}$ annihilation via h starts to dominate and the relic density enters the 3σ region again. For $m_S \sim m_h/2$, SS annihilation hits the h -pole, corresponding to the second dip around $m_S \sim 60$ GeV. The annihilation cross section gets smaller once m_S leaves the h -pole region. When $m_S \gtrsim 70$ GeV, $SS \rightarrow WW$ dominates. The annihilation cross section quickly increases and the relic density drops below the WMAP observed value.

The dashed and dot-dashed curves in the left plot of Fig. 2 shows the relic density dependence for $\delta_2=8$ GeV and 5 GeV respectively. Coannihilation effects get stronger for smaller mass splittings. Therefore, for most of the m_S region between 40 – 60 GeV, the coannihilation cross section is too large and the relic density is too small.

Curves in the right plot of Fig. 2 correspond to $\lambda_L=0.01, 0.1, 0.2, 0.3$ and 0.5 , respectively, while (δ_1, δ_2) is fixed to be $(50, 10)$ GeV. Similar Z -pole and h -pole features appear. The relic density is smaller for larger λ_L , since SS annihilation via h -exchange is increased due to the increased SSh coupling.

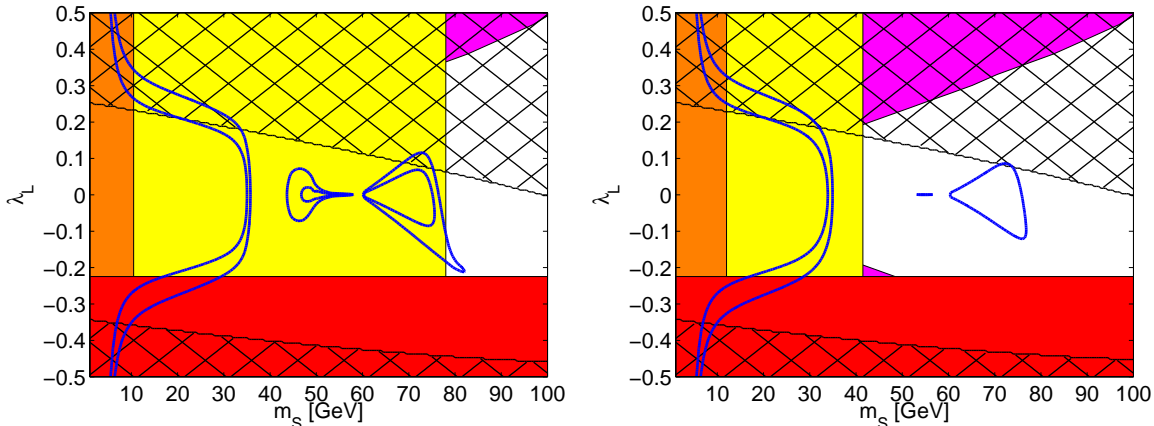


FIG. 3: WMAP 3σ allowed region (enclosed by blue curves) in $m_S - \lambda_L$ plane for $m_h=120$ GeV. The mass splittings are chosen to be $(\delta_1, \delta_2) = (50, 10)$ GeV (left plot) and $(50, 8)$ GeV (right plot). Shaded regions are excluded either by LEP I+II searches (yellow, light shade), electroweak precision constraints (orange, medium shade), dark matter direct detection (purple, medium-dark shade), vacuum stability (red, dark shade along bottom), and perturbativity (hatched region).

Fig. 3 shows the WMAP 3σ relic density allowed region (enclosed by two blue curves) in the $m_S - \lambda_L$ plane for $m_S < 100$ GeV with $m_h = 120$ GeV for $(\delta_1, \delta_2) = (50, 10)$ GeV (left plot) and $(50, 8)$ GeV (right plot). Shaded regions are excluded by various theoretical and experimental constraints, as described in Sec. III.

For $(\delta_1, \delta_2) = (50, 10)$ GeV (left plot), the gap around $m_S \sim 40$ GeV corresponds to the Z -pole. The gap around $m_S \sim 60$ GeV corresponds to the h -pole. The LEP constraint (yellow, light shade region) is very strong due to the strong constraints on m_A and m_S when $\delta_2 > 8$ GeV. The precision electroweak constraints (orange, medium shade region) is weak since $\delta_1 > \delta_2$ is slightly preferred by the fit to the $S - T$ contour. Given all the constraints, only a small region around $m_S \sim 80$ GeV survives. The value for λ_L for the allowed region, however, could be as large as -0.2 . Such a large value of λ_L would be important for generating a large signal in the indirect detection of dark matter.

The LEP constraints on m_S and m_A , however, are weakened for small mass splitting $\delta_2 \lesssim 8$ GeV. For such a small mass splitting, m_S as low as around 40 GeV is still allowed. In the right plot of Fig. 3, the allowed parameter space is given for $(\delta_1, \delta_2) = (50, 8)$ GeV. In

most of the m_S region between 40 GeV and 60 GeV, the relic density for the dark matter is too small due to the large coannihilation SA cross section. However, there is a viable region for $60 \text{ GeV} < m_S < 80 \text{ GeV}$ with λ_L in the region of ± 0.1 .

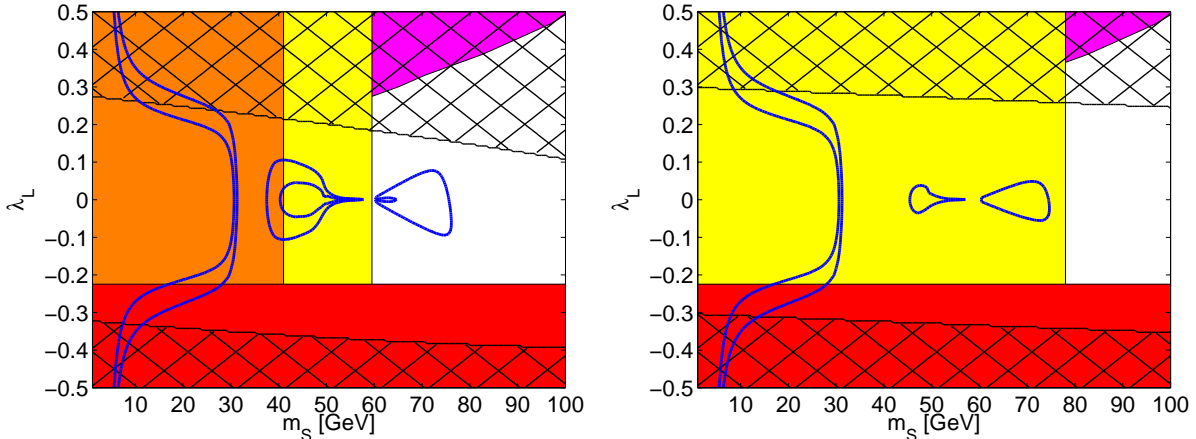


FIG. 4: WMAP 3σ allowed region (enclosed by blue curves) in $m_S - \lambda_L$ plane for $m_h=120$ GeV. The mass splittings are chosen to be $(\delta_1, \delta_2) = (10, 50)$ GeV (left plot), $(10, 10)$ GeV (right plot). Shaded regions are excluded by various theoretical and experimental constraints; see caption of Fig. 3 for explanation.

The left plot of Fig. 4 shows the allowed relic density region for $(\delta_1, \delta_2) = (10, 50)$ GeV and $m_h = 120$ GeV. The dark matter annihilation behaves similarly to the $(50, 10)$ case, only that the previous SA coannihilation via Z is replaced by SH^\pm coannihilation via W^\pm . The LEP constraints (yellow, light shade region) becomes weaker comparing to $(\delta_1, \delta_2) = (50, 10)$ GeV case, due to the weaker constraints on m_{H^\pm} . The precision electroweak constraints (orange, medium shade region), however, becomes stronger. Given all the theoretical and experimental constraints, a region with $60 \text{ GeV} < m_S < 80 \text{ GeV}$ and $-0.1 < \lambda_L < 0.1$ survives.

When δ_1 and δ_2 are both small, the coannihilations between S , A and H^\pm are relevant and the allowed 3σ regions shrink due to the enhanced coannihilation cross sections. For $(\delta_1, \delta_2) = (10, 10)$ GeV, there is no allowed region that survives given all the theoretical and experimental constraints, which is shown in the right plot of Fig. 4. For $\delta_2 \lesssim 8$ GeV, although the LEP II constraints is weaker, the WMAP 3σ region for $m_S > 40$ GeV completely disappears due to strong coannihilation effects.

Fig. 5 shows the allowed relic density region for $m_h = 120$ GeV when both $\delta_{1,2}$ are large: $(\delta_1, \delta_2) = (50, 50)$ GeV (left plot) and $(\delta_1, \delta_2) = (70, 70)$ GeV (right plot). The gaps in the low mass region corresponding to the Z -pole or W -pole disappear, since the mass splitting is too large for the coannihilation process to be important. The h -pole, however, still survives due to the low value of $m_h = 120$ GeV that we pick. The LEP I+II constraints (yellow, light shade region) are weaker because of the large value of δ_2 .

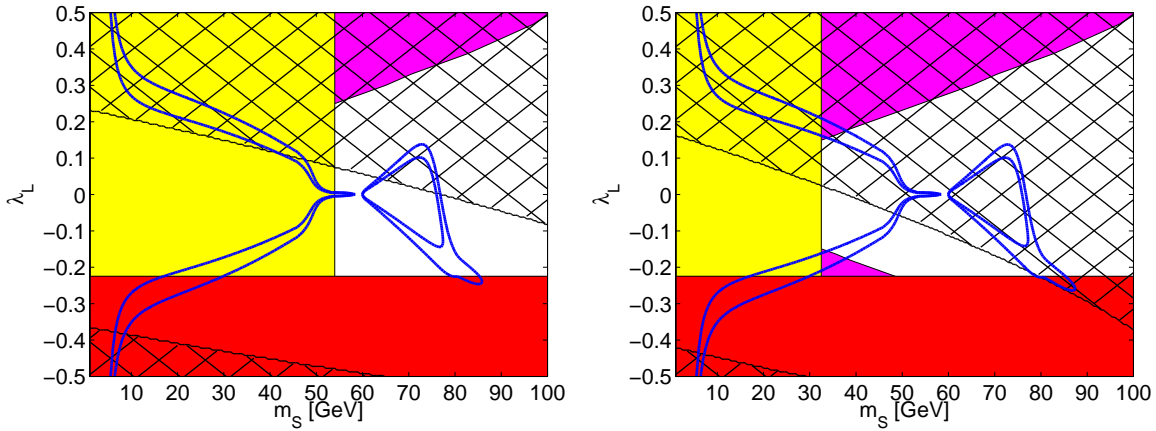


FIG. 5: WMAP 3σ allowed region (enclosed by blue curves) in $m_S - \lambda_L$ plane for $m_h=120$ GeV. The mass splittings are chosen to be $(\delta_1, \delta_2) = (50, 50)$ GeV (left plot), $(70, 70)$ GeV (right plot). Shaded regions are excluded by various theoretical and experimental constraints; see caption of Fig. 3 for explanation.

The perturbativity constraints (hatched region), however, are stronger, since larger mass splittings $\delta_{1,2}$ correspond to larger values for $\lambda_{4,5}$.

For splitting $(\delta_1, \delta_2) = (50, 50)$ GeV, a region with $55 \text{ GeV} < m_S < 90 \text{ GeV}$ and $-0.2 < \lambda_L < 0$ is consistent with the WMAP 3σ region. When the mass splittings get larger, the perturbativity constraint gets stronger (the hatched region shifts to the left) while the LEP II constraint gets weaker (the yellow, light shade region also shifts to the left). For $(\delta_1, \delta_2) = (70, 70)$ GeV, a region with $30 \text{ GeV} < m_S < 50 \text{ GeV}$ and $-0.15 < \lambda_L < -0.05$ opens up. For $(\delta_1, \delta_2) = (90, 90)$ GeV the perturbativity constraint is so strong that no mass window survives all of the constraints.

Fig. 6 shows the allowed relic density region for a high value of the SM Higgs mass $m_h = 500$ GeV. Electroweak precision constraints require a large value for δ_1 (as shown in Fig. 1) in order to compensate for the $\Delta S > 0$ and $\Delta T < 0$ contributions from a heavy SM Higgs. The left plot of Fig. 6 shows the allowed relic density region for $(\delta_1, \delta_2) = (250, 110)$ GeV. No pole regions appear due to the large mass splittings and large m_h . For $m_S \lesssim 75$ GeV, $SS \rightarrow b\bar{b}$ dominates, which corresponds to the nearly horizontal band of the 3σ WMAP region. Once $m_S \gtrsim 75$ GeV, $SS \rightarrow WW$ opens up, which leads to the nearly vertical band of the 3σ region. Dark matter with mass around 75 GeV is allowed given all of the constraints. Note that the perturbativity bounds are much weaker due to the large SM Higgs mass (therefore, large λ_1). On the other hand, to obtain the right relic density, large λ_L is needed to compensate the suppression of the annihilation cross section by the large Higgs mass m_h . Although λ_L could be as large as 3, the indirect detection in this region is not promising due to large suppression of the annihilation cross section by m_h^2 .

The numerical results do not change much for smaller values of δ_2 . A Z -pole coannihilation region appears for δ_2 around 10 GeV. The right plot of Fig. 6 shows the

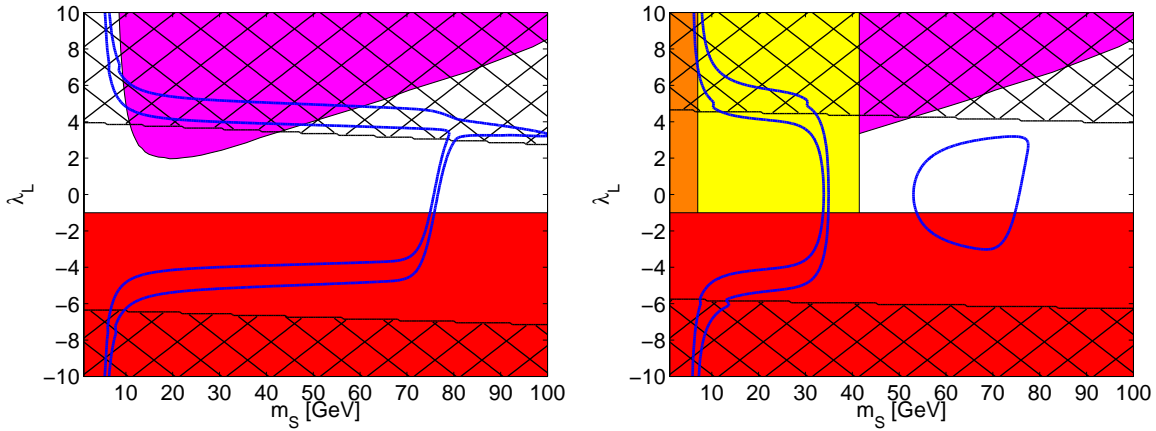


FIG. 6: WMAP 3σ allowed region (enclosed by blue curves) in $m_S - \lambda_L$ plane for $m_h=500$ GeV. The mass splittings are chosen to be $(\delta_1, \delta_2) = (250, 110)$ GeV (left plot), $(180, 8)$ GeV (right plot). Shaded regions are excluded by various theoretical and experimental constraints; see caption of Fig. 3 for explanation.

allowed relic density region for $(\delta_1, \delta_2) = (180, 8)$ GeV. The gap around $m_S \sim 40$ GeV is due to the Z -pole. The LEP II constraints on m_S and m_A do not apply, due to the small mass splitting. This allows a relatively large m_S region around $50 - 80$ GeV to remain open, with $-1 < \lambda_L < 3$. This region, however, shrinks for smaller δ_2 due to the stronger coannihilation effects. Therefore, no WMAP 3σ region survives for δ_2 less than about 6 GeV.

B. High mass region

Fig. 7 shows the relic density in the $m_S - \lambda_L$ plane for the high mass region: $m_S > 400$ GeV, with $m_h=120$ GeV. The LEP search bound is irrelevant now since the m_S is much larger than the direct search limit. The precision electroweak constraint is weak for m_h around 120 GeV as long as δ_1 and δ_2 do not differ too much. The dark matter direct detection constraint is also weak due to the heavy dark matter mass. For small mass splittings, $(\delta_1, \delta_2) = (1, 1)$ GeV (left plot in Fig. 7), a region of $m_S \sim 500 - 700$ GeV and $-0.2 < \lambda_L < 0.2$ is allowed. The dominating annihilation channels are WW , WZ and ZZ . The dependence on λ_L is introduced by the SSh coupling. For λ_L close to zero, a smaller value of m_S is preferred to increase the annihilation cross section. When $|\lambda_L|$ gets larger, a larger value of m_S is needed for the relic density to fall into the 3σ band. The region to the right of the 3σ band overclose the Universe while the region to the left of the 3σ band corresponds to the under-abundance region. Regions with large values of $|\lambda_L|$ are excluded due to the perturbativity constraints.

The annihilation cross section grows for large mass splittings. Therefore, the WMAP

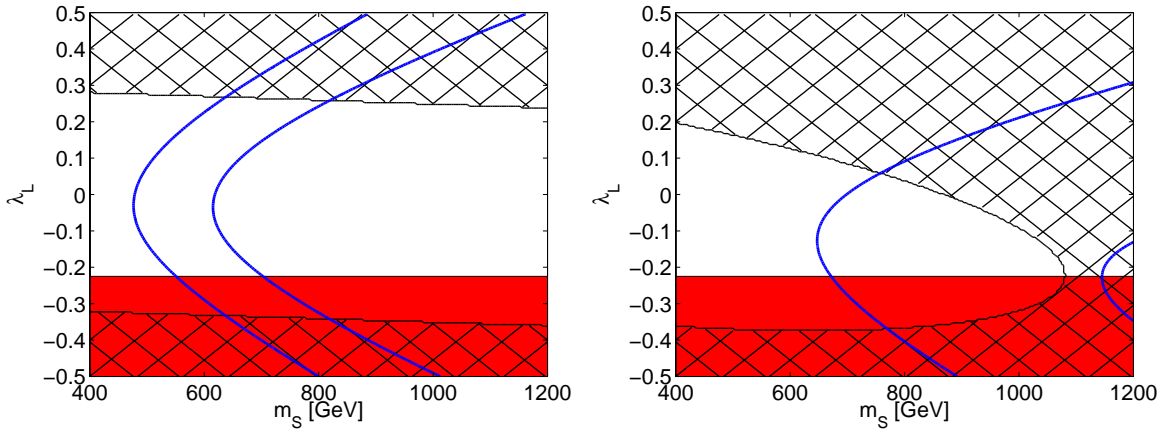


FIG. 7: WMAP 3σ allowed region (enclosed by blue curves) in $m_S - \lambda_L$ plane for $m_h=120$ GeV. The mass splittings are chosen to be $(\delta_1, \delta_2) = (1, 1)$ GeV (left plot), $(1, 10)$ GeV (right plot). Red region are excluded by vacuum stability while the hatched region are excluded by perturbativity constraints.

allowed region shifts to larger m_S for larger $\delta_{1,2}$, as shown in the right plot of Fig. 7 for $(\delta_1, \delta_2) = (1, 10)$ GeV. $m_S \gtrsim 650$ GeV falls into the WMAP 3σ region. The result for $(\delta_1, \delta_2) = (10, 1)$ GeV is very similar. The region forbidden by perturbativity constraints (hatched region), however, shifts to the left for larger $\delta_{1,2}$. Therefore, no allowed region is left if at least one of $\delta_{1,2} \gtrsim 12$ GeV.

For a large SM Higgs mass $m_h = 500$ GeV, a large mass splitting $\delta_1 \gtrsim 150$ GeV is needed to satisfy the precision electroweak constraints. There is no region in $m_S - \lambda_L$ that survives after all of the experimental and theoretical constraints are taken into account.

V. CONCLUSION

We studied the simple extension of the SM Higgs sector when an extra inert Higgs doublet is introduced that couples to the gauge sector only. The lighter of the neutral components could be a good WIMP dark matter candidate. We explored the parameter spaces of the IHDM, taking into account the relic density constraints from WMAP and various theoretical and experimental constraints. Table I summarizes five distinctive regions that could provide the right amount of cold dark matter in the Universe which satisfy all of the constraints.

In regions (I) – (IV), the dark matter candidate S , along with at least one of the other scalars A, H^\pm is light. Those particles could be pair produced at the Large Hadron Collider (LHC) as SA, AH^\pm, SH^\pm and H^+H^- with cross sections around the fb level. Heavier scalars A and H^\pm could decay into the lightest one S via on-shell(or off-shell) $Z^{(*)}$ and $W^{(*)}$, which further decay into quarks, leptons and neutrinos. There are typically large

		m_h	m_S (GeV)	λ_L	δ_1, δ_2
(I)	light dark matter	low m_h	30 – 60	–0.15 to 0	$50 \text{ GeV} \lesssim \delta_1 \sim \delta_2 \lesssim 90 \text{ GeV}$
(II)			60 – 80	–0.2 to 0.2	at least one of δ_1, δ_2 is large
(III)		high m_h	50 – 75	–1 to 3	large δ_1 and small $\delta_2 < 8 \text{ GeV}$
(IV)			~ 75	–1 to 3	large δ_1 and δ_2
(V)	heavy dark matter	low m_h	500–1000	–0.2 to 0.3	small $\delta_{1,2}$

TABLE I: Allowed parameter regions in the IHDM that are consistent with the WMAP dark matter relic density 3σ region.

missing E_T in those processes due to the undetectable S particles which are at the end of the decay chains. Experimentally, we can search for events with single lepton + missing E_T , dilepton + missing E_T , trilepton + missing E_T or in general, jets + leptons + missing E_T . The dominant SM background comes from WW , WZ and ZZ . The collider analysis on this model is currently under study [37]. The scalar mass in the high mass region (V), however, is larger than 500 GeV. Since they only have weak interactions, the production cross section at the LHC is typically too small.

For the low m_h region (II), when a relatively large $|\lambda_L| \sim 0.2$ could be accommodated, the indirect detection of the dark matter via its annihilation into neutrinos, photons, electrons and positrons could be very promising. A recent study on the indirect neutrino signals [14] showed that in the low m_S region, tens to a hundred of neutrino events per year from dark matter annihilation inside the Earth and hundreds of neutrino events per year from dark matter annihilation inside the Sun can be expected at future neutrino telescopes. Indirect photon signals including monochromatic photon line, fragmentation photon spectrum and final state radiation photon spectrum in the IHDM is under current study [38]. High m_h regions (III) and (IV) typically don't have promising indirect detection signals due to the suppression of the annihilation cross section by large m_h . The indirect detection possibility for the high m_S region (V) is also less comparing to region (II). In Ref. [14], it is shown that neutrino events from the Earth is too low to be observed, while a few events per year is expected from neutrinos from the sun.

In summary, the IHDM is a simple extension of the SM which provides a very promising WIMP dark matter candidate. There are several regions of the parameter space that could provide the right amount of dark matter relic density in the Universe. The collider phenomenology of this model is very rich. For certain regions, the indirect detection via neutrinos or photons is possible at future neutrino and gamma ray telescopes or ground based experiments.

Acknowledgments

We would like to thank B. Thomas for useful discussion and comments. This work is supported under U.S. Department of Energy contract# DE-FG02-04ER-41298.

-
- [1] D. N. Spergel *et al.* [WMAP Collaboration], *Astrophys. J. Suppl.* **148**, 175 (2003).
 - [2] G. Servant and T. M. P. Tait, *Nucl. Phys. B* **650**, 391 (2003) [arXiv:hep-ph/0206071].
 - [3] V. Silveira and A. Zee, *Phys. Lett. B* **161**, 136 (1985);
 - [4] J. McDonald, *Phys. Rev. D* **50**, 3637 (1994) [arXiv:hep-ph/0702143];
 - [5] C. P. Burgess, M. Pospelov and T. ter Veldhuis, *Nucl. Phys. B* **619**, 709 (2001) [arXiv:hep-ph/0011335].
 - [6] N. G. Deshpande and E. Ma, *Phys. Rev. D* **18**, 2574 (1978);
 - [7] R. Barbieri, L. J. Hall and V. S. Rychkov, *Phys. Rev. D* **74**, 015007 (2006);
 - [8] Z. Chacko, H. S. Goh and R. Harnik, *JHEP* **0601**, 108 (2006);
 - [9] E. Ma, *Phys. Rev. D* **73**, 077301 (2006);
 - [10] T. Hambye and M. H. G. Tytgat, *Phys. Lett. B* **659**, 651 (2008) [arXiv:0707.0633 [hep-ph]].
 - [11] M. Lisanti and J. G. Wacker, arXiv:0704.2816 [hep-ph].
 - [12] E. Ma, *Mod. Phys. Lett. A* **21**, 1777 (2006) [arXiv:hep-ph/0605180]; T. Hambye, K. Kannike, E. Ma and M. Raidal, *Phys. Rev. D* **75**, 095003 (2007) [arXiv:hep-ph/0609228].
 - [13] L. Lopez Honorez, E. Nezri, J. F. Oliver and M. H. G. Tytgat, *JCAP* **0702**, 028 (2007).
 - [14] P. Agrawal, E. M. Dolle and C. A. Krenke, *Phys. Rev. D* **79**, 015015 (2009) [arXiv:0811.1798 [hep-ph]].
 - [15] S. Andreas, M. H. G. Tytgat and Q. Swillens, arXiv:0901.1750 [hep-ph].
 - [16] M. Gustafsson, E. Lundstrom, L. Bergstrom and J. Edsjo, *Phys. Rev. Lett.* **99**, 041301 (2007) [arXiv:astro-ph/0703512].
 - [17] E. Nezri, M. H. G. Tytgat and G. Vertongen, arXiv:0901.2556 [hep-ph].
 - [18] D. Majumdar and A. Ghosal, *Mod. Phys. Lett. A* **23**, 2011 (2008) [arXiv:hep-ph/0607067].
 - [19] E. Lundstrom, M. Gustafsson and J. Edsjo, arXiv:0810.3924 [hep-ph].
 - [20] Q. H. Cao, E. Ma and G. Rajasekaran, *Phys. Rev. D* **76**, 095011 (2007) [arXiv:0708.2939 [hep-ph]].
 - [21] W. M. Yao *et al.*, *Journal of Physics G* **33**, 1 (2006) and 2007 partial update for edition 2008 available on the PDG WWW pages (URL: <http://pdg.lbl.gov/>).
 - [22] LEP Higgs Working Group for Higgs boson searches, arXiv:hep-ex/0107031; J. Abdallah *et al.* [DELPHI Collaboration], *Eur. Phys. J. C* **34**, 399 (2004).
 - [23] A. Abulencia *et al.* [CDF Collaboration], *Phys. Rev. Lett.* **96**, 042003 (2006).
 - [24] A. Pierce and J. Thaler, *JHEP* **0708**, 026 (2007) [arXiv:hep-ph/0703056].
 - [25] The LEP SUSY working group, <http://lepsusy.web.cern.ch/lepsusy/>, LEPSUSYWG/01-03.1.
 - [26] The LEP Electroweak Working Group, <http://lepewwg.web.cern.ch/LEPEWWG/>
 - [27] M. E. Peskin and T. Takeuchi, *Phys. Rev. D* **46**, 381 (1992).

- [28] J. Angle *et al.* [XENON Collaboration], Phys. Rev. Lett. **100**, 021303 (2008)
- [29] Z. Ahmed *et al.* [CDMS Collaboration], Phys. Rev. Lett. **102**, 011301 (2009)
- [30] Sarah Andreas, Michel H. G. Tytgat, and Quentin Swillensy, JCAP **0904**, 004 (2009)
- [31] D. S. Akerib *et al.* [CDMS Collaboration], Phys. Rev. D **68**, 082002 (2003)
- [32] G. Angloher *et al.* [CRESST Collaboration], Astropart. Physics **18**, 43 (2002)
- [33] C. E. Aalseth *et al.* [CoGeNT Collaboration], Phys. Rev. Lett. **101**, 251301 (2008)
- [34] S. T. Lin *et al.* [TEXONO Collaboration], Phys. Rev. D **79**, 061101 (2009)
- [35] G. Blanger, F. Boudjema, A. Pukhov, A. Semenov, Comput.Phys.Commun.176:367-382,2007; hep-ph/0607059; G. Belanger, F. Boudjema, A. Pukhov and A. Semenov, arXiv:0803.2360 [hep-ph].
- [36] <http://theory.sinp.msu.ru/~pukhov/calchep.html>.
- [37] E. M. Dolle, X. Miao, S. Su and B. Thomas, in preparation.
- [38] E. M. Dolle, S. Su, in preparation.